Correction Procedures for the Numerical Parasitic Elements Associated with Lumped Elements in Global Electromagnetic Simulators

Raphaël Gillard, Stéphane Dauguet, and Jacques Citerne

***Abstract*— This paper presents a comparative study of the treatment of lumped elements in two different full-wave electromagnetic formulations: the finite-difference time-domain (FDTD) technique and the technique of integral equations. Although these two approaches are basically different, they are seen to exhibit the same kind of numerical troubles when lumped elements are involved. More precisely, lumped elements are systematically associated with numerical parasitic elements that can seriously alter the calculated results. As a solution, this paper proposes a general alternative formulation, which permits one to suppress these numerical parasites. This formulation is successfully applied to the FDTD technique. A simpler numerical deembedding procedure, which does not fundamentally transform the original formulation, is preferred for the integral-equation technique.**

***Index Terms*— Finite-difference time-domain, integral equations, lumped-circuit element, numerical deembedding.**

I. Introduction

THE global electromagnetic analysis of complex active printed circuits and antennas appears as the only means of taking all couplings and radiations into account. As a preliminary step, several attempts have been made to include lumped-circuit elements in so-called global electromagnetic simulators. Among these, the three-dimensional (3-D) finite-difference time-domain (FDTD) formulation has been extended in order to enable the modeling of the connection of linear and nonlinear lumped elements [1], [2]. The technique of integral equations associated with the method of moments and the theory of loaded scatterers has also been demonstrated to provide a powerful means of modeling simple active microstrip antennas [3] and circuits [4]. Similar results have been reported using the finite-element method (FEM) [5]. All these methods appear as hybrid approaches, as they combine Maxwell equations for the passive distributed part of the circuit and Kirchhoff equations for the active lumped part. Unfortunately, lumped elements do not permit one to take the actual dimensions of the component they represent into account. Moreover, they are usually associated with numerical parasitic elements that can dramatically spoil the results [6].

The main goal of this paper is to propose an improved modeling to represent discrete elements in electromagnetic simulations. This paper first discusses the traditional way of introducing lumped elements in the FDTD technique and focus on the resultant parasites. As a solution, a new formulation is proposed that relies on the equivalence principle and uses fictitious magnetic-current densities. This formulation not only permits one to represent the actual size of the inserted components, it also reduces the numerical parasitic elements. The paper then discusses the easiest way of modeling lumped elements in the method of moments. Although the formulation is quite different, it is demonstrated that it leads to similar numerical parasites. In that case, numerical deembedding procedures are proposed, which permit one to suppress these parasitic elements without requiring a total review of the original formulation.

II. Lumped-Circuit Elements in the FDTD Technique

A. The Classical Formulation and Its Parasitic Elements

The FDTD method has been demonstrated to be particularly well suited to study planar loaded circuits. As a 3-D method, it provides a convenient way of modeling complex structures. As a time-domain method, it provides a natural representation for nonlinear phenomena. Two main approaches have been proposed to connect discrete elements across FDTD cells. The first one is analogous to the microscopic approach, as it involves an exact description of the different materials constitutive of the component [7]. Although this approach is theoretically more rigorous, it can only be applied to elementary components with simple descriptions, and will not be discussed here. The second method is a lumped approach, which uses an electrical equivalent circuit to represent the discrete element [1], [2]. This is illustrated in Fig. 1 for the simple case of a standard Yee cell loaded by a resistive voltage source. Classically, the generator can be taken into account by adding a lumped current density $\vec{J}_L$ to the second hand of the Maxwell–Ampere curl equation

$$\vec{\nabla} \times \vec{H} = \varepsilon \frac{\partial}{\partial t} \vec{E} + \vec{J}_L. \tag{1}$$

Manuscript received January 20, 1998; revised March 13, 1998.

R. Gillard and J. Citerne are with LCST/INSA, UPRES A CNRS 6075 20, 35043 Rennes Cedex, France.

S. Dauguet was with LCST/INSA, UPRES A CNRS 6075 20, 35043 Rennes Cedex, France. He is now with the Society Celwave, Lanion 22, France.

Publisher Item Identifier S 0018-9480(98)06164-X.

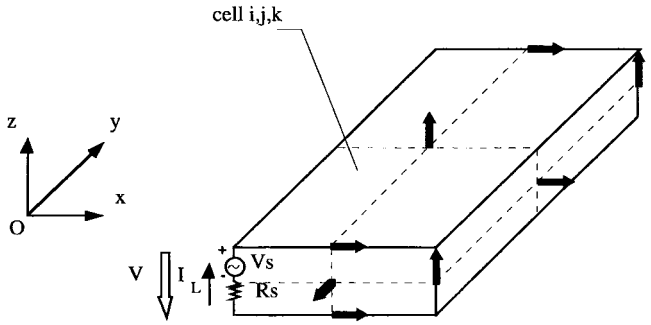

Fig. 1. Standard Yee cell with a lumped resistive voltage generator.

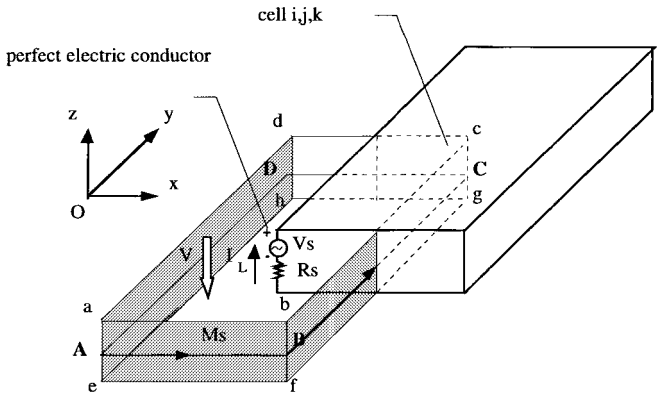

Fig. 2. Magnetic-current representation.

This additional current density results from the lumped current I_L flowing in the generator

$$\vec{J}_L = \frac{I_L}{\Delta x \Delta y}\vec{e}_z. \tag{2}$$

It can be related to the voltage across the loaded FDTD cell

$$V = -V_s + R_s I_L. \tag{3}$$

Unfortunately, the actual size and precise location of the component cannot easily be taken into account, and cumbersome distributing procedures may be required [9].

Moreover, as shown in (1), the total current density flowing across the loaded cell consists of a displacement current density in addition to the lumped current density. As a consequence, a parasitic capacitance is connected in parallel with the lumped element. This capacitance is that of the loaded cell [6]

$$C_L = \frac{\varepsilon \Delta z}{\Delta x \Delta y}. \tag{4}$$

It is present because the lumped element occupies only one wedge of the cell: it lies along the z-wedge of the cell, but has no transverse dimensions. One important characteristic of this capacitance is that its value is strongly dependant from the spatial meshing. As a consequence, it should be seen as a numerical parasitic capacitance with no physical significance. Moreover, it has been demonstrated that this capacitance can spoil the results [6].

B. The Alternative Formulation

This paper proposes an alternative formulation. It consists of replacing all the volume occupied by the component by its electrical equivalent circuit. As a consequence, it takes into account the actual size of the component and suppresses the parasitic capacitance of the loaded cells. However, it remains versatile and general since it relies on an equivalent-circuit approach. Basically, this approach uses the equivalence principle to represent the discrete element by a fictitious magnetic-current density. This magnetic current surrounds the volume occupied by the component and simulates the voltage across its terminals. As a result, it produces the same fields outside the volume and zero fields inside it, which permits to vanish the effect of the inner FDTD cells.

This formulation is presented for the lumped generator, shown in Fig. 1. Using the principle of equivalence, an external equivalent problem can be obtained by assuming a perfect conductor inside volume $abcdefgh$ and by adding a horizontal magnetic current M_s on the vertical part of its surface, as shown in Fig. 2, and as follows:

$$\vec{M}_s = -\vec{n} \times \vec{E}. \tag{5}$$

In this equation, the voltage across the resistive source generates the electric field, which is responsible for the surface magnetic current

$$\vec{E} = \frac{V}{\Delta z}\vec{e}_z. \tag{6}$$

In order to account for this magnetic current, the general form of the Maxwell–Faraday curl equation has to be used for time-stepping the magnetic field

$$\vec{\nabla} x \vec{E} = -\vec{M}_s - \mu \frac{\partial}{\partial t}\vec{H}. \tag{7}$$

Using central difference in combination with (5) and (6) to update $H_{x,i,j,k}$ leads to

$$\frac{E_z|^{n+1/2}_{i,j+1,k} - E_z|^{n+1/2}_{i,j,k}}{\Delta y} - \frac{E_y|^{n+1/2}_{i,j,k+1} - E_y|^{n+1/2}_{i,j,k}}{\Delta z} = \frac{V^{n+1/2}}{\Delta y \Delta z} - \mu \frac{H_x|^{n+1}_{i,j,k} - H_x|^{n}_{i,j,k}}{\Delta t}. \tag{8}$$

The voltage V is given by Ohm's law applied to the generator as in (3), where the current I_L can be expressed as the circulation of the magnetic field around the path $ABCD$

$$I_L^{n+1/2} = (H_x|^{n+1/2}_{i,j-1,k} - H_x|^{n+1/2}_{i,j,k})\Delta x + (H_y|^{n+1/2}_{i,j,k} - H_y|^{n+1/2}_{i-1,j,k})\Delta y. \tag{9}$$

Theoretically, this expression involves three components of the magnetic field, in addition to the one to be updated. Unfortunately, these components must be known at step $n+1/2$, which is not compatible with the usual iterative scheme. In [8], we proposed an approximate formulation for (9) that uses a semi-implicit form only for the updated component

$$I_L^{n+1/2} \approx \left(H_x|^{n}_{i,j-1,k} - \frac{H_x|^{n+1}_{i,j,k} + H_x|^{n+1}_{i,j,k}}{2}\right)\Delta x + (H_y|^{n}_{i,j,k} - H_y|^{n}_{i-1,j,k})\Delta y. \tag{10}$$

However, it results in cumbersome expressions that cannot easily be generalized to more complex discrete elements. Moreover, it can lead to instabilities when the impedance of the lumped element is very large.

In this paper, we propose a simpler procedure. We assume that the electric-current density is uniform in the volume occupied by the discrete element. This is coherent with the fact that we use a macroscopic representation of this element (the equivalent circuit). As a consequence, the tangential component of the magnetic field is constant all around the lateral surface of this element, which means

$$H_{x\,i,\,j-1,\,k}^{\,n+1/2} = -H_x|_{i,\,j,\,k}^{n+1/2} = H_y|_{i,\,j,\,k}^{n+1/2} = -H_y|_{i-1,\,j,\,k}^{n+1/2}. \quad (11)$$

Finally, when computing (8), I_L can be related only to the updated magnetic-field component

$$I_L^{n+1/2} = -(H_x|_{i,\,j,\,k}^{n+1} + H_x|_{i,\,j,\,k}^{n})(\Delta x + \Delta y) \quad (12)$$

and we obtain

$$\begin{aligned} H_x|_{i,\,j,\,k}^{n+1} &= \frac{\dfrac{\mu}{\Delta t} - R_s\dfrac{(\Delta x+\Delta y)}{\Delta y\Delta z}}{\dfrac{\mu}{\Delta t} + R_s\dfrac{(\Delta x+\Delta y)}{\Delta y\Delta z}} H_x|_{i,\,j,\,k}^{n} - \frac{1}{\dfrac{\mu}{\Delta t} + R_s\dfrac{(\Delta x+\Delta y)}{\Delta y\Delta z}} \\ &\quad \cdot \left[\frac{E_z|_{i,\,j+1,\,k}^{n+1/2} - E_z|_{i,\,j,\,k}^{n+1/2}}{\Delta y} - \frac{E_y|_{i,\,j,\,k+1}^{n+1/2} - E_y|_{i,\,j,\,k}^{n+1/2}}{\Delta z}\right] \\ &\quad - \frac{\dfrac{V_s^{n+1/2}}{\Delta y\Delta z}}{\dfrac{\mu}{\Delta t} + R_s\dfrac{(\Delta x+\Delta y)}{\Delta y\Delta z}}. \end{aligned} \quad (13)$$

Similar equations can be obtained to update $H_{x,\,i,\,j-1,\,k}$, $H_{y,\,i,\,j,\,k}$ and $H_{y,\,i-1,\,j,\,k}$ by replacing (12) with an equivalent relation involving the component that is to be updated.

In addition to these equations, $E_{z,\,i,\,j,\,k}$ has to be forced to zero in order to respect the perfect conductor condition inside volume $abcdefgh$ as follows:

$$E_z|_{i,\,j,\,k} = 0. \quad (14)$$

Also, in order to insure stability, (11) has to be enforced *a posteriori* by averaging all the involved components of the magnetic field before the next time step

$$\begin{aligned} H_x|_{i,\,j-1,\,k}^{n+1} &= -H_x|_{i,\,j,\,k}^{n+1} = H_y|_{i,\,j,\,k}^{n+1} = -H_y|_{i-1,\,j,\,k}^{n+1} \\ &= \frac{H_x|_{i,\,j-1,\,k}^{n+1} - H_x|_{i,\,j,\,k}^{n+1} + H_y|_{i,\,j,\,k}^{n+1} - H_y|_{i-1,\,j,\,k}^{n+1}}{4}. \end{aligned} \quad (15)$$

This formulation can be generalized to deal with a generator extending over N cells along x. The global electric current flowing through the N loaded cell is calculated as the circulation of the magnetic field along the path, as shown in Fig. 3. In addition, the H_y and the E_x components located between two loaded cells have to be forced to zero as they now lie inside the perfect conductor. The main advantage of this treatment is that it implies no assumption concerning the horizontal distribution of the vertical current.

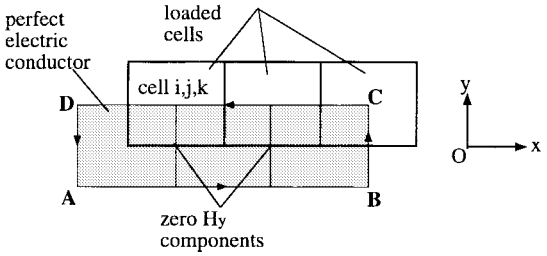

Fig. 3. Three loaded-cell configuration.

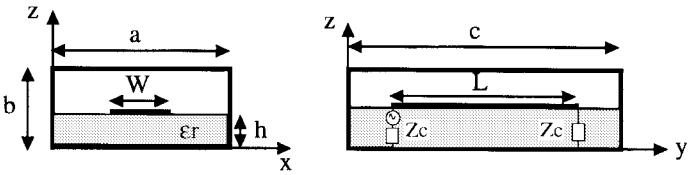

Fig. 4. Studied structure: ($a = 1.778$ mm, $b = 1.27$ mm, $c = 25.4$ mm, $L = 22.606$ mm, $h = 0.254$ mm, $W = 0.254$ mm, $\varepsilon_r = 9.8$, $Z_c = 45\Omega$).

The formulation can also be generalized to analyze reactive elements. As an illustration, we give the expressions that would be obtained for a series *RL* circuit

$$V^{n+1/2} = R\frac{I_L^n + I_L^{n+1}}{2} + \frac{L}{\Delta t}\frac{I_L^{n+1} - I_L^n}{2} \quad (16)$$

and for a shunt *RC* circuit

$$V^{n+1/2} = \frac{\Delta t}{C}\sum_{m=0}^{n} I_L^{m+1/2} e^{(m-n)\Delta t/RC}. \quad (17)$$

As a first illustration, a shielded microstrip line excited by a matched generator at its first extremity and terminated by a matched load at the other one is studied (see Fig. 4). In this example, the discrete matched loads are used in order to avoid complex absorbing boundary conditions, as in [10]. The meshing involves 35 cells in the x-direction, 100 cells in the y-direction, and 25 cells in the z-direction. The time step is 0.11 ps and 4545 iterations are performed. The width of the line extends over five cells, which requires a distribution of the discrete elements along x. A first simulation [see Fig. 5(a)] was performed using the classical lumped-element formulation. The obtained return loss is equal to that produced by a matched load with a 15-fF shunt capacitance. This value is exactly that of the terminal capacitance of the open-ended line, which was computed in a previous FDTD simulation. A second simulation [see Fig. 5(b)] was achieved using the magnetic-current formulation. The return loss is equivalent for low frequencies, but much better for higher frequencies (7 dB lower at 20 GHz). In this case, using (14), no displacement current can flow through the loaded cells, which means the corresponding capacitances vanish. As a result, the total parasitic capacitance at the end of the line decreases. The evaluation of the remaining capacitance gives 10 fF. This simple example confirms that the parasitic capacitance associated with the very loaded cells has been suppressed.

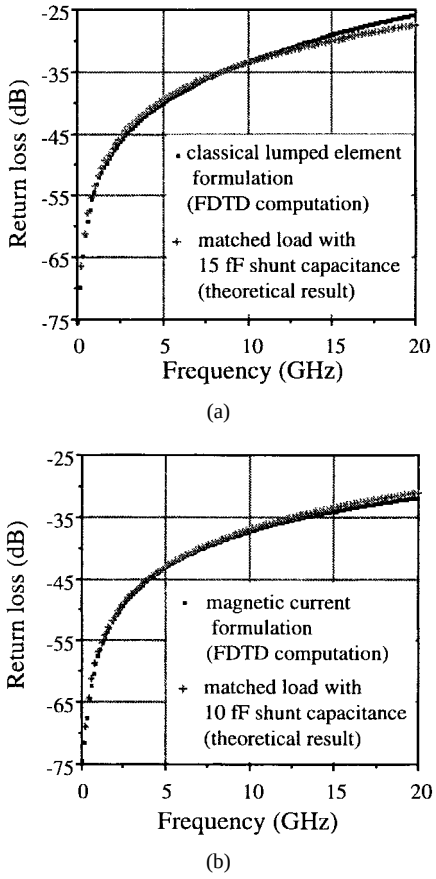

Fig. 5. Return loss versus frequency. (a) Classical formulation. (b) Magnetic-current formulation.

As a second example, we present the simulation of a thick-film chip resistor inserted in a microstrip line. The studied structure is depicted in Fig. 6. Two different modelings have been tested and compared to measured data [7]. The first modeling uses an exact description of the inner structure of the discrete component [7]. The second modeling, the one that is proposed in this paper, replaces this description with an electric equivalent circuit that occupies exactly the same volume in the FDTD mesh. The meshing involves 65 cells in the x-direction, 275 cells in the y-direction, and 30 cells in the z-direction. The time step is 0.22 ps and 1636 iterations are performed. As no equivalent circuit was available, we first built a simple one. As shown in Fig. 6, it involves a series inductance L and a shunt capacitor C. L accounts for the parasitic inductive effect of the two vertical electrodes and of the horizontal resistive sheet: its value was computed by simulating an air bridge with the same dimensions (the resistive sheet was simply replaced with a metallic conductor). C accounts for the capacitive coupling between the two vertical electrodes: its value was computed by simulating these two electrodes alone (the resistive sheet was simply removed). It must be noticed that these additional simulations will usually not be necessary since equivalent circuits are supposed to be provided with discrete components. As in [7], we performed the simulations for two different values of the resistance. The results are shown in Fig. 7. For the 10-Ω resistance, we used (16), which means we neglected the capacitive element in the equivalent circuit. For the 820-Ω resistance, we used (17), which means we neglected the inductive element in the equivalent circuit. Although the equivalent circuit is rather coarse, the obtained results are seen to be in good agreement with both the measurements and exact description. All these results are much better than those computed in [7] using the classical formulation for lumped elements. We believe that these latter results could be improved by using the equivalent circuit we proposed instead of a simple planar resistance. Nevertheless, the problem of the numerical parasitic capacitance would remain. In any case, this example demonstrates the capability of our modeling to represent 3-D discrete components using an equivalent-circuit representation. It appears as a powerful alternative to the exact description, especially for complex circuits for which both a very fine meshing and a set of complex physical equations would be required.

III. Lumped Elements Using the Method of Moments

A. The Classical Formulation and Its Parasitic Elements

The theory of loaded scatterers was introduced by Harrington [11] to analyze one-port serial lumped loads embedded in wire antennas, using the technique of integral equations. It has recently be generalized to perform the global electromagnetic analysis of printed antennas [3] and circuits [4] involving active two-port elements connected to ground. The general formulation will be recalled in the simple case of a perfectly conducting microstrip line loaded with a lumped impedance Z_L (see Fig. 8). The line is supposed to be fed with a matched generator and terminated with a matched load. These matched terminations can easily be inserted in the formulation as described in [12] and will not be presented here. Despite this, the discussion will focus on the treatment of the lumped impedance and, more precisely, on the associated numerical parasitic elements. The fundamental assumption of the theory of loaded scatterers consists of stating that the impedance Z_L is located in a zero length gap G_L [see Fig. 9(a) and (b)]. This permits one to considerably simplify the electromagnetic analysis, as it requires no interruption of the perfect electric conductors supporting the lumped element. Unfortunately, it will be shown that it can result in severe numerical disorders.

Classically, the integral equation expresses the cancellation of the total tangential electric field at the surface of the perfect electric conductors

$$\vec{e}_z \times [\vec{E}^{\text{inc}}(\vec{r}_i) + \vec{E}^{\text{diff}}(\vec{r}_i)] = \vec{0} \tag{18}$$

where $\vec{E}^{\text{inc}}$ is the incident electric field, $\vec{E}^{\text{diff}}$ is the diffracted electric field, and $\vec{r}_i$ is an observer point on the metallizations.

The diffracted electric field can be written in terms of mixed potentials

$$\vec{E}^{\text{diff}}(\vec{r}_i) = -j\omega\vec{A}(\vec{r}_i) - \vec{\nabla}V(\vec{r}_i) \tag{19}$$

with

$$\vec{A}(\vec{r}_i) = \iint_S \overline{\overline{G}}_A(\vec{r}_i, \vec{r}_\nu)\vec{J}_s(\vec{r}_\nu)\, dS_\nu \tag{20}$$

and

$$V(\vec{r}_i) = \iint_S G_V(\vec{r}_i, \vec{r}_\nu)\rho_s(\vec{r}_\nu)\, dS_\nu. \tag{21}$$

In these expressions, $\overline{\overline{G}}_A$ and G_V are the exact dyadic and scalar dielectric multilayer Green functions of the structure,

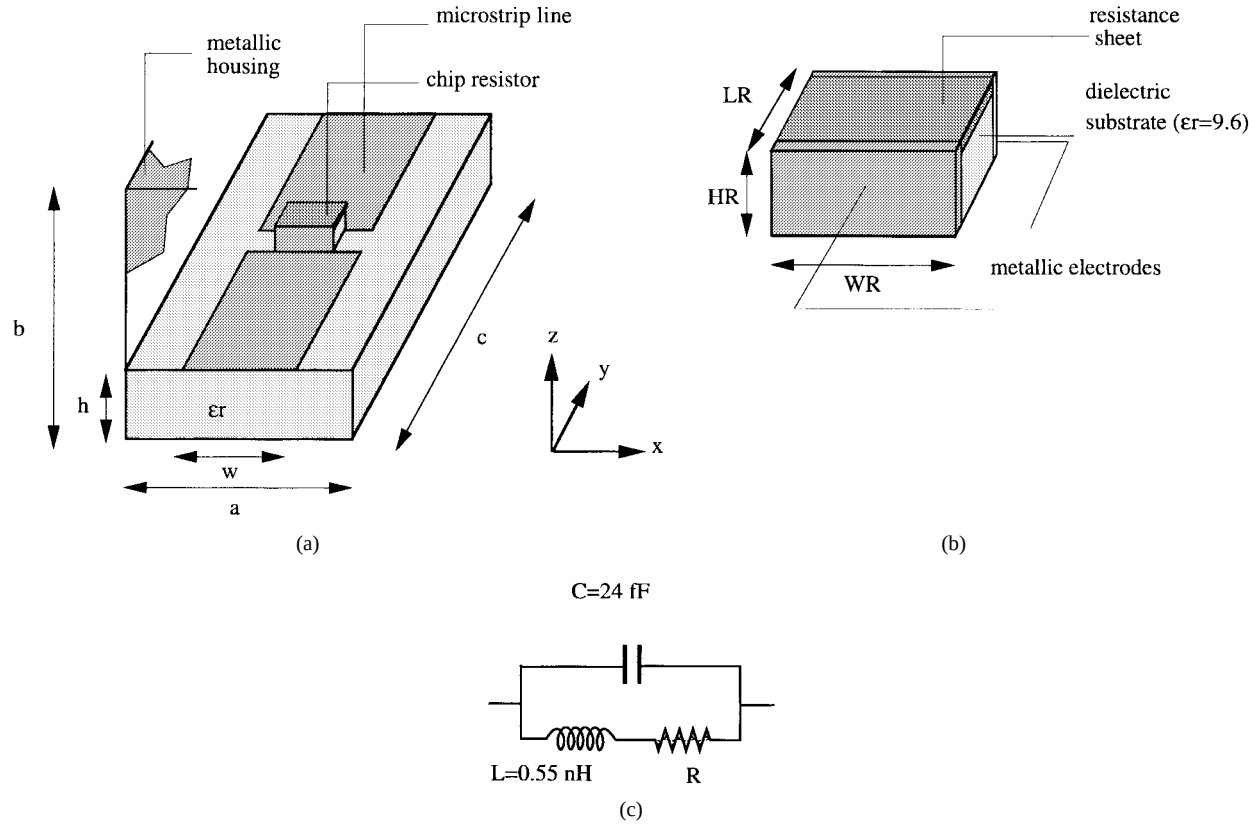

Fig. 6. Studied structure. (a) The loaded microstrip line ($a = 6.578$ mm, $b = 3.048$ mm, $c = 55.653$ mm, $\varepsilon_r = 2.2$, $h = 0.508$ mm, $w = 1.518$ mm). (b) The thick-film chip resistor ($WR = 1.214$ mm, $HR = 0.508$ mm, $LR = 4.047$ mm). (c) The equivalent circuit.

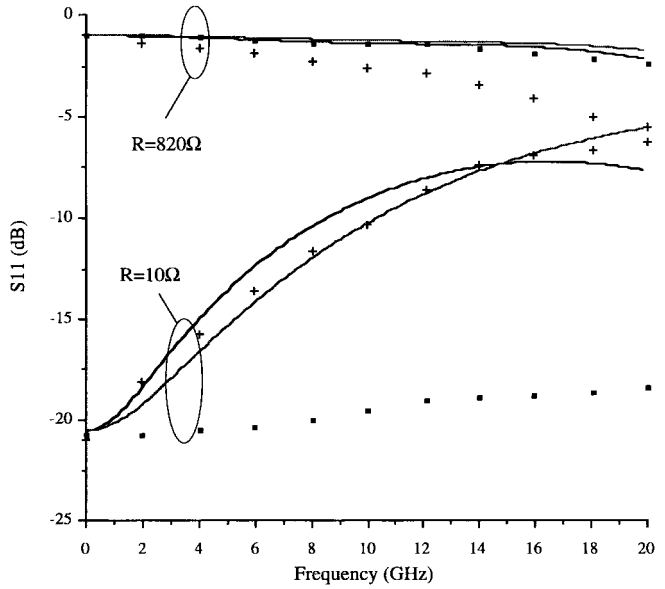

Fig. 7. Return loss versus frequency for different modelings. —: this analysis. ∞∞: exact description [7]. +: measurements [7]. ■: [7].

$\vec{J}_s$ and ρ_s are the electric current and charge densities, and $\vec{r}_\nu$ is a source point at the surface S of the metallizations.

Inserting (21) and (20) into (19) and then into (18) gives

$$\vec{E}^{\text{inc}}(\vec{r}_i) \times \vec{e}_z = \left[j\omega \iint_S \overline{\overline{G}}_A(\vec{r}_i, \vec{r}_\nu) \vec{J}_s(\vec{r}_\nu)\, dS_\nu + \vec{\nabla} \iint_S G_V(\vec{r}_i, \vec{r}_\nu) \rho_s(\vec{r}_\nu)\, dS_\nu \right] x\vec{e}_z. \quad (22)$$

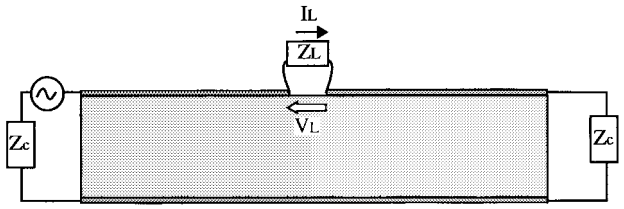

Fig. 8. Studied structure.

The theory of loaded scatterers assumes that the incident field is zero everywhere, except at the location of the infinitesimal gap G_L where it represents the voltage V_L across the lumped element

$$\vec{E}^{\text{inc}}(\vec{r}_i) = \begin{cases} V_L \vec{e}_x, & \text{if } \vec{r}_i \in G_L \\ 0, & \text{elsewhere} \end{cases} \quad (23)$$

$$V_L = Z_L I_L. \quad (24)$$

The electric current flowing through the gap I_L can be related to the longitudinal current density across the gap

$$I_L = \int_0^{W_L} \vec{J}_s(x_L, y, 0) \cdot \vec{e}_x\, dy \quad (25)$$

where x_L is the x-coordinate of the gap and W_L is its width.

It must be understood that, in our formulation, the actual source is not represented by the incident field, but by additional boundary conditions applied to the current densities [12].

This integral equation (22) can be solved using the method of moments. In this paper, we used the same formulation as in [13], i.e., rectangular cells, rooftop basis functions, and test

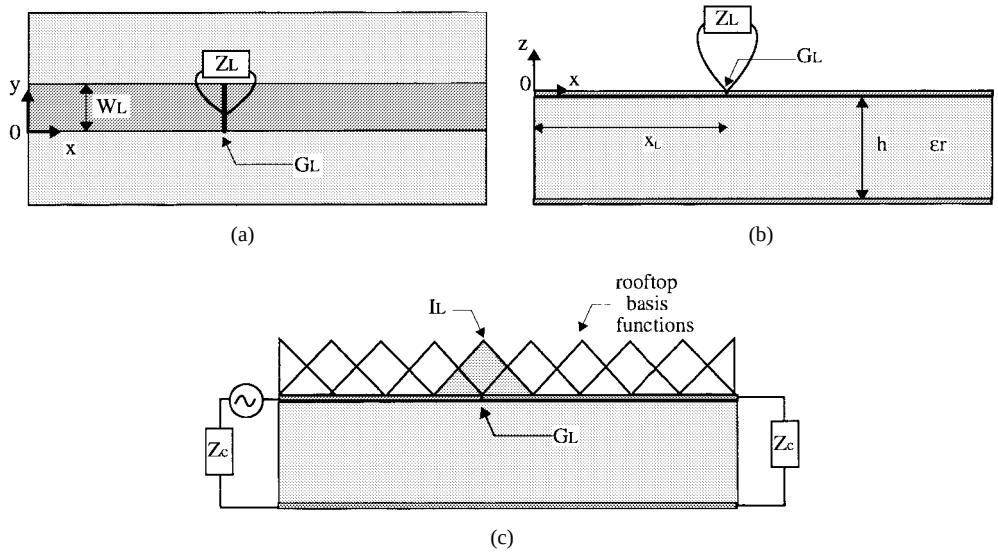

Fig. 9. Numerical representation of the studied structure ($h = 0.8$ mm; $\varepsilon_r = 2.17$, $W_L = 2.47$ mm, $f = 8$ GHz). (a) Top view. (b) Front view. (c) Front view with basis functions.

segments. Practically, the gap G_L is located at the border between two successive cells and the current I_L is given by the top value of the corresponding rooftop basis function [see Fig. 9(c)].

Although very attractive, this formulation has a major drawback: the zero-length gap G_L is associated with an infinite susceptance. This can be understood very easily, as it corresponds to the limit of a nonzero-length gap (with a finite susceptance) whose length tends to zero. As a consequence, the gap behaves as an infinite capacitance and the current flowing through it is singular. Fortunately, the actual numerical situation is not so bad. Thanks to the smoothing achieved by the basis function expansion, the current calculated at the location of the gap does not become infinite. This means the capacitance does not get infinite either. However, the remaining capacitance C_L is strongly dependent from the meshing (the looser the meshing is, the larger the smoothing and the smaller the capacitance). Here again, it must be regarded as a numerical parasitic capacitance whose presence cannot be accepted. In that case, we can note that the parasitic capacitance is due to the zero length of the lumped element and not to its zero transverse dimensions as in the FDTD technique.

Fig. 10 (noncorrected results) illustrates the effect of the numerical parasitic capacitance when a lumped resistance R_L is inserted in a microstrip line. The figure presents the simulated impedance Z_L^{sim} for different values of the inserted resistance R_L. Z_L^{sim} is the resultant serial impedance that actually appears at the location of the gap; it is deduced from the calculated scattering parameters of the loaded gap. As long as R_L remains small, the effect of the shunt capacitance is negligible and Z_L^{sim} faithfully reproduces the value of R_L. When R_L gets larger, the shunt capacitance becomes more influent and Z_L^{sim} exhibits a significant capacitive behavior. Fig. 11 reports the variations of the numerical parasitic capacitance C_L for different meshings and for several line configurations (the procedure used to compute C_L will be explained later). As expected, C_L is strongly dependent on the mesh size and is smaller for looser meshing. It also appears that C_L is larger for wider lines, which is consistent with the fact that the coupling is stronger.

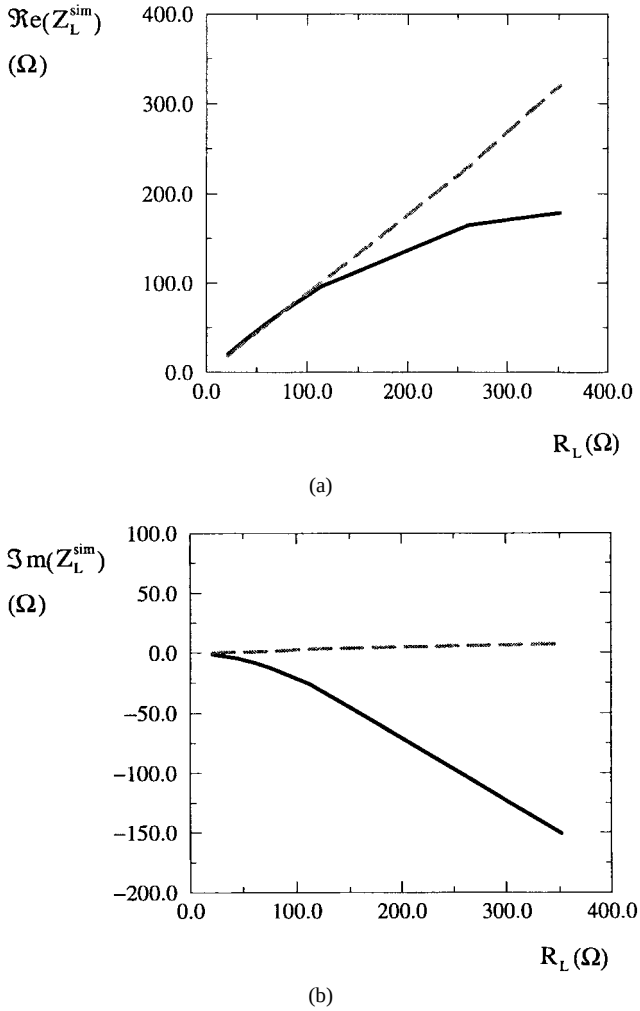

Fig. 10. Simulated impedance versus inserted resistance. —: noncorrected results. – –: corrected results (first deembedding procedure). (a) Real part. (b) Imaginary part.

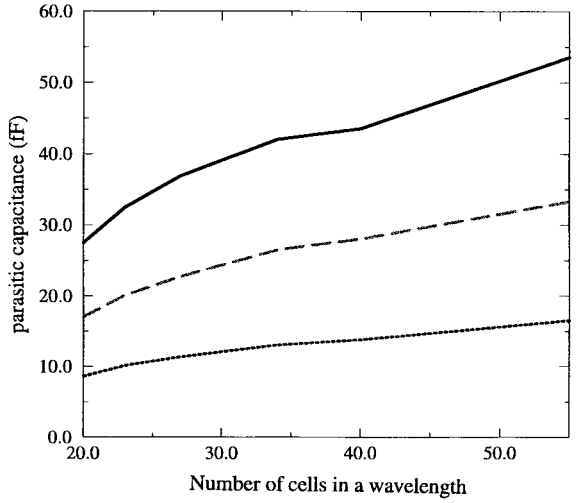

Fig. 11. Numerical parasitic capacitance for different mesh sizes. —: $W_L = 2.47$ mm. – –: $W_L = 1.65mm$. - - - -: $W_L = 0.82$ mm.

B. The Deembedding Procedures

From the theoretical viewpoint, the theory of loaded scatterers relies on a poor assumption that is responsible for this problem; at the same time, it assumes a zero total electric field and a nonzero incident electric field at the location of the discrete element. Indeed, the voltage due to this element should be contained in the total electric field and not in the incident electric field. In practice, this could be achieved by using a zero total electric field (this is necessary to obtain a simple boundary condition for the integral equation) and by adding a magnetic current to represent the voltage due to the discrete element. Unfortunately, this rigorous modeling, which has been chosen for the FDTD technique in the previous section, is not so easy to implement for the technique of integral equations. Practically, it would need the calculation of vertical and horizontal magnetic Green functions in order to account for the contribution of the magnetic current surrounding the discrete element.

As a consequence, this paper proposes two alternative solutions. They can be seen as a numerical deembedding procedures. These two complementary solutions will be discussed for the situation depicted in Fig. 8.

The first one relies on the fact that the numerical error due to the parasitic capacitance is a systematic one; when the capacitance is known, this error can be predicted and corrected. As previously seen, the value of the capacitance is perfectly deterministic once the mesh size is fixed. As a consequence, the procedure first determines the value of the capacitance for the chosen meshing. To do so, the microstrip line is simulated with an infinite lumped impedance Z_L inserted in the gap G_L. This loading configuration corresponds to that of the parasitic capacitance alone (as it lies in parallel with an infinite impedance). Its value can be so derived from the resulting scattering parameters

$$C_L = \frac{1}{j\omega Z_c}\Im m\left[\frac{2S_{21}}{(1+S_{11})^2 - S_{21}^2}\right]. \tag{26}$$

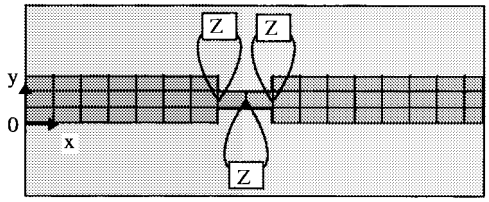

Fig. 12. Improved numerical representation of the studied structure. $Z = Z_L/3$.

In (26), the scattering parameters and the characteristic impedance of the line Z_c can be computed as in [12]. Once the capacitance is known, its effect can be removed for all the following simulations. Typically, the correction simply consists of inserting a compensated impedance Z_L^{comp} when an impedance Z_L is to be simulated as follows:

$$Z_L^{\text{comp}} = \frac{Z_L}{1 - j\omega C_L Z_L}. \tag{27}$$

This procedure completely cancels the effect of the infinitesimal gap, as shown in Fig. 10 (corrected results). Nevertheless, although it produces robust numerical results, this technique presents a major drawback—it does not account for the actual physical gap supporting the discrete element.

The second solution provides a more realistic description of the actual connection conditions. Indeed, it not only permits one to suppress the parasitic effect of the infinitesimal gap, it also permit one to include the effect of the physical gap. This solution combines a precise modeling of the actual gap, a distribution of the lumped element, and a revisited deembedding procedure. As shown in Fig. 12, the lumped element is divided into N serial elements Z_L/N situated along a narrow metallic strip in the gap ($N = 3$ in Fig. 12). In practice, the width and length of this strip have to be adjusted to correspond to those of the actual discrete element. This is essential when the analysis software is to be coupled with an auto-layout procedure. The first advantage of this modeling is its ability to reduce the effect of the parasitic capacitance. As previously demonstrated, the capacitance gets smaller when the infinitesimal gap becomes more narrow, which is the case here. In addition, as the value of the lumped elements themselves are smaller (Z_L/N instead of Z_L), the presence of a small parallel capacitance is not important anymore, and it is not necessary to correct it. The second advantage results from the realistic treatment of the physical gap. Typically, when Z_L is infinite, the current completely disappears along the narrow metallic strip (due to the shape and interlacing of the basis functions) and the physical gap is reconstructed. The only drawback of this approach is that it uses a nonphysical narrow metallic strip, which is supposed to introduce a parasitic inductive effect. In order to avoid this problem, a deembedding procedure is used. It consists of computing the parasitic inductance in a first simulation (it can be deduced from the scattering parameters of the narrow metallic strip alone, as with the capacitance). This serial parasitic inductance is then removed from all the following simulations.

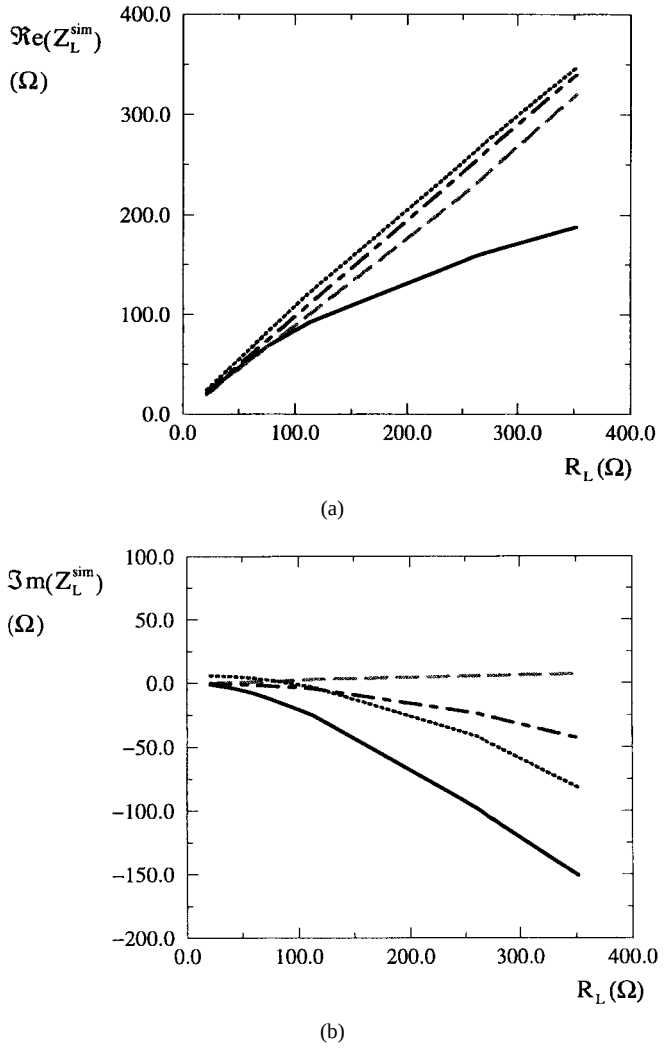

Fig. 13. Simulated impedance versus inserted resistance. —: noncorrected results (first deembedding procedure). – –: corrected results (first deembedding procedure). - - - -: corrected results (second deembedding procedure). – - -: HP EESOF results. (a) Real part. (b) Imaginary part.

Fig. 13 illustrates the effect of this procedure. Here again, it presents the value of the simulated impedance for different inserted resistances. Three different configurations are tested: the first one is obtained by inserting the resistance in an infinitesimal gap without any correction, the second one uses the first deembedding procedure, and the third one uses the second deembedding procedure. These three different configurations are compared with the results produced by performing the shunt connection of the resistance and gap in a circuit simulator (HP EESOF). For such a simple structure, the circuit simulator can be regarded as a reference. As expected, the first deembedding configuration exhibits no capacitive effect at all. The noncorrected configuration exhibits a significant capacitive effect, larger than the one resulting from the physical gap. Moreover, as seen previously, this effect would be largely dependent on the mesh size. The second deembedding configuration is very similar to the circuit simulator, which demonstrates its validity.

As an illustration, Fig. 14 presents a microstrip-patch antenna loaded with two varactor diodes. This antenna can

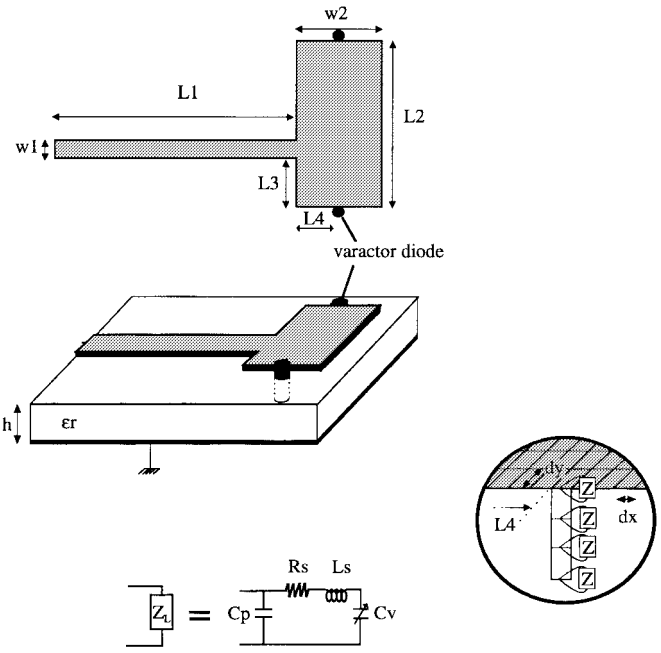

Fig. 14. The studied frequency-agile microstrip antenna and its numerical modeling $L1 = 75$ mm, $W1 = 4.61$ mm, $L2 = 41.5$ mm, $W2 = 27$ mm, $L3 = 13.83$ mm, $L4 = W2/2$, $h = 1.6$ mm, $\varepsilon_r = 2.17$, $d_x = 1$ mm, $d_y = 4.61$ mm, $R_s = 1\Omega$, $L_s = 0.4$ nH, $C_p = 0.13$ pF.

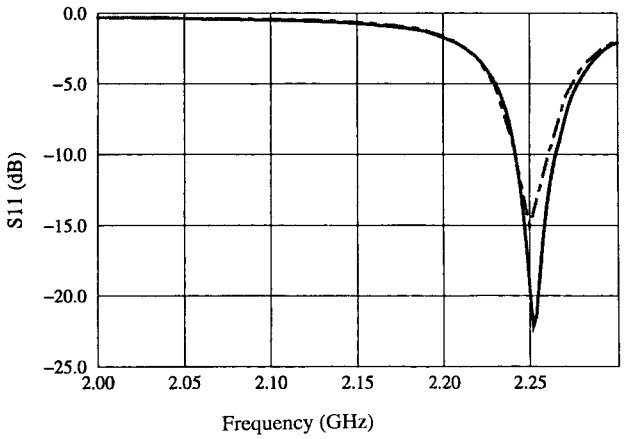

Fig. 15. Variations of the return loss versus frequency for $C_v = 0.5$ pF. —: measurement. - - - -: theory.

operate as a frequency-agile element since the dc bias applied to the diodes controls their capacitance. This structure has been analyzed using the second deembedding procedure. The diodes (MA4ST553-120) were modeled by using the equivalent circuit given in the constructor data sheet. The results shown in Fig. 15 are those obtained for $C_v = 0.5$ pF. The same agreement has been obtained for other values of the bias. Such a global electromagnetic analysis is particularly suitable for this structure, in which the discrete elements are really embedded in the radiating element.

IV. Conclusion

In this paper, the presence of numerical parasitic capacitances associated with lumped elements in global electromagnetic simulations has been demonstrated. These capacitances

have been shown to result from the lumped elements themselves (lumped elements with no transverse dimensions in the FDTD technique and with no longitudinal dimensions in the technique of integral equations). The common property of these capacitances are their strong dependency in regards to the mesh size, which definitively classes them as numerical parasites. A general alternative formulation has been proposed to deal with discrete elements. It uses the equivalence principle to replace all the volume occupied by a discrete element by its equivalent electric circuit. This formulation has been successfully applied to the FDTD technique. Although it could also be used in the integral-equation formulation, it would lead to cumbersome developments. As a consequence, deembedding procedures are preferred in that case. These procedures have been seen to be particularly suitable for frequency-domain methods, and their efficiency has been demonstrated.

REFERENCES

[1] W. Sui, D. A. Christensen, and C. H. Durney, "Extending the two-dimensional FDTD method to hybrid electromagnetic systems with active and passive lumped elements," *IEEE Trans. Microwave Theory Tech*, vol. 40, pp. 724–730, Apr. 1992.

[2] M. Piket-May, A. Taflove, and J. Baron, "FDTD modeling of digital signal propagation in 3-D circuits with passive and active loads," *IEEE Trans. Microwave Theory Tech.*, vol. 42, pp. 1514–1523, Aug. 1994.

[3] R. Gillard, H. Legay, J. M. Floc'h, and J. Citerne, "A rigorous analysis of a receiving active microstrip antenna," *Electron. Lett.*, vol. 27, no. 25, pp. 2357–2359, Dec. 1991.

[4] S. Daughet, R. Loison, R. Gillard, J. Citerne, and G. Piton, "Rigorous global electromagnetic analysis of interconnections in MHIC applications," *Electron. Lett.*, vol. 32, no. 17, pp. 1596–1597, Aug. 1996.

[5] K. Guillouard, M. F. Wong, V. F. Hanna, and J. Citerne, "A new global finite element analysis of microwave circuits including lumped elements," in *IEEE MTT-S Symp. Dig*, San Francisco, CA, June 1996, pp. 355–358.

[6] O. P. M. Pekonen and J. Xu, "Rigorous analysis of circuit parameter extraction from an FDTD simulation excited with a resistive voltage generator," *Microwave Opt. Technol. Lett.*, vol. 12, no. 4, pp. 205–210, July 1996.

[7] Y. C. Lau, M. S. Leong, and P. S. Kooi, "Modeling of chip resistors for high-frequency microwave applications with the use of the FDTD method," *Microwave Opt. Technol. Lett.*, vol. 14, no. 5, pp. 259–261, Apr. 1997.

[8] R. Gillard, K. Moustadir, F. Lebolzer, and J. Citerne, "A magnetic current formulation for modeling discrete components using the FDTD method," in *IEEE MTT-S Symp. Dig.*, Denver, CO, June 1997, pp. 71–74.

[9] C. H. Durney, W. Sui, D. A. Christenses, and J. Zhu, "A general formulation for connecting sources and passive lumped-circuits elements across multiple 3-D FDTD cells," *IEEE Microwave Guided Wave Lett.*, vol. 6, pp. 85–87, Feb. 1996.

[10] J. B. Verdu, R. Gillard, K. Moustadir, and J. Citerne, "An extension of the PML technique to the FDTD analysis of multilayer planar circuits and antennas," *Microwave Opt. Lett.*, vol. 10, no. 6, pp. 323–327, Dec. 1995.

[11] R. F. Harrington, "The theory of loaded scatterers," *Proc. Inst. Elect. Eng.*, vol. 111, no. 4, pp. 617–623, Apr. 1964.

[12] R. Gillard, J. H. Corre, M. Drissi, and J. Citerne, "A general treatment of matched terminations using integral equations—Modeling and applications," *IEEE Trans. Microwave Theory Tech.*, vol. 42, pp. 2545–2553, Dec. 1994.

[13] J. R. Mosiga and F. G. Gardiol, "General integral equation formulation for microstrip antennas and scatterers," *Proc. Inst. Elect. Eng.* vol. 132, pt. H, no. 7, pp. 424–432, Dec. 1985.

Raphaël Gillard was born June 11, 1966, in France. He received the Diplôme d'Ingénieur and Ph.D. degree in electronics from the National Institute of Applied Sciences (INSA), Rennes, France, in 1989 and 1992, respectively.

From 1992 to 1993, he was an Engineer at the Society IPSIS, where he worked on commercial electromagnetic simulators. In 1993, he joined the Microwave Group, INSA, as an Associate Professor. His current research interest concerns numerical methods applied to the computer-aided design (CAD) of microwave circuits and active antennas.

Stéphane Dauguet was born in Fougéres, France, in 1969. He received the Diplôme d'Ingénieur and the Ph.D. degree in electronics from the National Institute of Applied Sciences (INSA), Rennes, France, in 1993 and 1997, respectively. His doctoral research topic dealt with global electromagnetic simulators for the study of active planar structures.

In 1997, he joined the Society Celwave, and is currently an Antenna Engineer in charge of the development of new products for base-station antennas in cellular networks.

Jacques Citerne was born in France on October 5, 1945. He received the Doctorate degree in physics from the University of Lille, France, in 1978.

Until 1981, he was Head of the Circuits and Propagation Group, Microwave and Semiconductor Center, Technical University of Lille. Since 1981, he has been a Professor of electrical engineering at the INSA, Rennes, France, where he has been responsible for the Laboratory for Telecommunication Components and Systems (LCST), which is supported by the French National Center of Scientific Research (CNRS), since 1984. The activities of LCST concern microwave and millimeter-wave circuits and antennas, indoor communications, spread spectrum systems, radar, and diffraction.